Journal of Nuclear Materials 406 (2010) 230–237

Contents lists available at ScienceDirect

Journal of Nuclear Materials

journal homepage: www.elsevier.com/locate/jnucmat

Reduction of selenite and selenate on anoxically corroded iron and the synergistic effect of uranyl reduction

Anders Puranen [a,*], Mats Jonsson [a], Rainer Dähn [b], Daqing Cui [c]

[a] KTH Chemical Science and Engineering, Nuclear Chemistry, Royal Institute of Technology, Se 100 44 Stockholm, Sweden
[b] Laboratory for Waste Management, Paul Scherrer Institut, Villigen CH-5232, Switzerland
[c] Hot Cell Laboratory, Studsvik Nuclear AB, 71182 Nyköping, Sweden

ARTICLE INFO

Article history:
Received 29 April 2009
Accepted 25 August 2010

ABSTRACT

In this work the uptake of dissolved selenium in the form of selenite and selenate on iron covered by a magnetite corrosion layer and the effect of dissolved uranyl on this process is studied. Under simulated anoxic groundwater conditions (bicarbonate and chloride solutions) no immobilization of selenate was found in the absence of uranyl whereas selenite was immobilized, albeit slowly. When uranyl was present, it was found to become reduced and greatly enhanced the rate of reductive immobilization of the dissolved selenite as well as selenate. The increased rate of immobilization is proposed to be due to the oxidative transformation of the passifying magnetite layer as the uranyl is reduced with the observed formation of a transient mixed Fe(II)/Fe(III) oxyhydroxide phase. The iron oxide, and selenium speciation on the surfaces were investigated by Raman spectroscopy. X-ray Absorption Spectroscopy was used to determine the oxidation state of the selenium and uranium on the surfaces.

1. Introduction

Release of the anthropogenic ^{79}Se isotope, which exists as a fission product in spent nuclear fuel (SNF), is a concern due to its β-activity and long half-life (in the range of 10^5–10^6 y, most recently reported at 3.27×10^5 y [1]). Although the amount of ^{79}Se in SNF is small (fission yield <0.05% [2]) the long half life of ^{79}Se, combined with its potentially high mobility and bioavailability makes it one of the key concerns in the long term safety assessment for a SNF repository. Se is a highly redox-sensitive element which can occur in a large span of geochemically relevant oxidation states; the soluble oxyanions selenate, Se(VI), SeO_4^{2-} and selenite, Se(IV), SeO_3^{2-}, elemental Se, with a rich allotropy and the selenides, Se(−II), which commonly form sparingly soluble minerals [3]. Many SNF repository designs such as the Swedish KBS-3 [4] rely on burial of the SNF in canisters deep under ground (∼500 m below the surface) where the conditions are expected to be anoxic. In most of the SNF repository designs a large part of the SNF-canister is composed of iron, sometimes with additional engineered barriers such as an outer copper canister and bentonite clay (as in the KBS-3 concept). In order for the SNF to be exposed to the groundwater the canister must fail with time. The iron will thereby come in contact with anoxic groundwater and corrode before the SNF matrix can release fission products, such as ^{79}Se. Iron and certain iron corrosion products have been shown to reduce and immobilize dissolved selenite and selenate [5–11]. Magnetite, Fe_3O_4 is believed to be a likely major corrosion product formed on iron corroding under anoxic groundwater conditions [12,13]. Studies have shown that selenite sorption on magnetite decreases with increasing pH with selenate following the same trend, albeit being less readily adsorbed [14], which is unfavorable at the expected pH of ∼8 in carbonate rich groundwater. The situation is somewhat unclear as to whether selenite is reduced by magnetite. Recent work by Scheinost et al. [10,11] employing synthetic nanoparticulate magnetite under anoxic conditions demonstrated reduction of selenite to ironselenide phases at a pH of ∼5. However, equally recent work also employing synthetic nanoparticulate magnetite under anoxic conditions indicated no reduction of adsorbed selenite in the pH range of 4.8–7.9 [15].

Since SNF is generally composed of ∼95% UO_2, a large amount of uranium will undergo at least some degree of dissolution in order for the SNF matrix to release significant amounts of fission products such as Se. The effect of the presence of uranyl on the immobilization of Se is consequently of interest, especially given that uranyl hydroxide or carbonate complexes can be reductively immobilized by iron [16,17], magnetite [18], and other iron corrosion products, such as green rusts, GR [19].

The studied system is not only of interest in a deep SNF repository context but also share similarities with other nuclear waste forms such as tank or pond wastes from past reprocessing activities. Another related issue is pollution from uranium mining tailings, which among the major contaminants such as uranium also

* Corresponding author. Tel.: +46 87909279; fax: +46 87908772.
E-mail address: puranen@kth.se (A. Puranen).

0022-3115/$ - see front matter © 2010 Elsevier B.V. All rights reserved.
doi:10.1016/j.jnucmat.2010.08.031

contains naturally occurring Se in levels of concern [20,21]. These wastes are often disposed in or expected to migrate into areas where the conditions are anoxic, with iron being a common major element in containers or engineered so called reactive permeable barriers [22] installed in order to remediate contaminant release.

As we have recently shown [23], reduction of dissolved uranyl has a strong impact on the immobilization of selenate by an iron surface. In the present study we examine the impact of dissolved uranyl on the immobilization of selenite and selenate by corroded iron surfaces with magnetite layers under simulated anoxic groundwater conditions.

Surface characterization was performed using Raman spectroscopy, Scanning Electron Microscopy Energy Dispersive X-ray Spectroscopy (SEM-EDS) and X-ray Absorption Spectroscopy (XAS).

2. Materials and methods

Iron foils (Goodfellow 99.75%-Fe), 20 μm thick were cut inside a glovebox (<0.1 ppm O_2) and polished to expose a fresh surface. The foils were then washed in distilled water to remove the polishing residues. They were divided so that several small pieces gave a total geometrical surface area ~4 cm^2 per sample. The polished foils were slightly bent to prevent them from laying flat on the bottom of a glass vessel which was filled with deoxygenated distilled water and sealed. The vessel was insulated and kept at 80 °C inside the glove box for 60 days. Iron powder (99.5% Fe, 140 μm diameter, Höganäs AB were also precorroded in the same manner as the iron foils. After a few days a shiny black corrosion layer started to appear on the precorrosion samples. Small subsamples of the precorroded materials were examined by Raman spectroscopy to identify the corrosion products and by SEM to investigate the thickness of the corrosion layer.

2.1. Batch experiments

Plastic bottles with 50 ml starting solution were used for the iron foil experiments. For the experiments with precorroded iron powder clear glass tubes were used to facilitate the observation of the evolution of the corrosion products. The standard solution was composed of 10 mM NaCl, 2 mM $NaHCO_3$ yielding pH ~8. All solutions were prepared inside the glove box (<0.1 ppm O_2, Ar + 0.03% CO_2) from degassed Milli-Q deionized water (18 MΩ). Uranylnitrate (Kebo, Pro analysi) was used to prepare the uranyl solutions. The selenite used (Na_2SeO_3, Alfa Aesar, 99.8%) was analyzed iodometrically (in the absence of oxygen) to test the selenite content which matched that of the ICP analysis indicating no selenate contamination of the selenite. The selenate (Na_2SeO_4, Alfa Aesar, 99.8%) was also analyzed iodometrically for selenite, of which none was found. The redox potential of the solutions was measured in the glove box using a Pt electrode and a Metrohm Ag/AgCl reference electrode that was verified using saturated quinhydrone buffers at pH 4 and 7. Aliquots were centrifuged (25,000*g*, 5 min) prior to any air exposure and the supernatant was analysed by Inductively Coupled Plasma Optical Emission Spectrometry (ICP-OES). The conditions for the selenite and selenate batch experiments are presented in Table 1.

Table 1
The first number in the sample name indicates the initial concentration and selenium speciation, the second number gives the initial uranyl concentration.

Sample	Se [μm]	U–VI [μm]
250SeIV	250SeIV	–
250SeVI	250SeVI	–
250SeIV/420U	250SeIV	420
250SeVI/420U	250SeVI	420

2.2. X-ray spectroscopy

Micro-XAS spectroscopy and fluorescence microprobe mapping was performed at the micro-XAS beamline at the Swiss Light Source (SLS) [24]. The beam size was ~2 × 6 μm^2. Commercial liquid sodiumselenate, selenite, solid gray elemental Se and ferroselite were used as Se references. For uranium, uranyl and UO_2 references were used. Prior to transport to the beamline the sample was sealed (in the glovebox) in a double air tight container with freshly regenerated oxygen scavenging copper pellets in the outer compartment of the container. The colour of the copper pellets indicated no intrusion of oxygen prior to the XAS-analysis. Multiple μ-XANES spectra were recorded for each region of interest and the first and last of each series was compared to check for possible redox reactions induced by the high photon flux of the synchrotron beam, of which no indication was found. The U or Se in the dried and encapsulated samples did not appear to be sensitive to oxidation by air or by redox effects while being handled at the beamline over the course of a few days and repeated beam exposures. Data averaging (three to five spectra from each spot), background correction and normalization were performed in the program WINXAS [25]. All spectra were collected at room temperature.

2.3. Raman microscopy

Samples were dried and sealed by kapton tape under a cover glass and transferred out of the glove box for immediate investigation by Raman microscopy. A Renishaw 1000 system with a 633 nm Spectra Physics model 127 laser was used. For the iron powder experiments a Renishaw inVia Reflex Raman microscope with a 532 nm laser was used. The spectra were recorded at room temperature using 20× and 80× magnification, corresponding to a spatial resolution of 5 μm or less. In order to avoid sample degradation the light was filtered down to a spot intensity of ~0.5 mW or less. Cosmic ray suppression was employed.

3. Results and discussion

3.1. Characterization of the preoxidized layers

The Raman spectra obtained for the precorroded material used in this work are shown in Fig. 1. The major band at 670 cm^{-1} agree with reported data for magnetite [26] indicating magnetite as the dominating species on the precorroded surfaces. Approximately

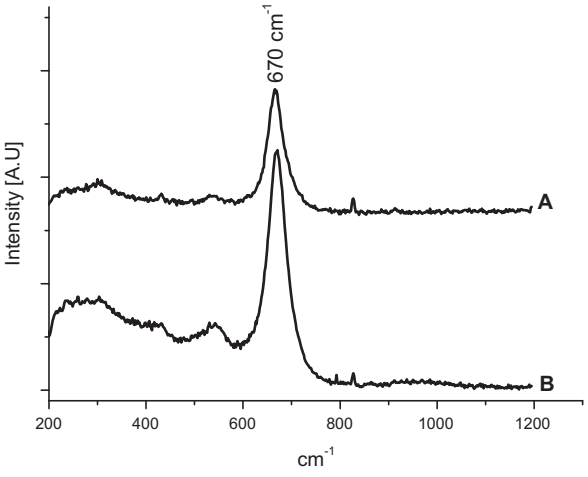

Fig. 1. Raman spectra. A: Magnetite reference. B: Precorroded iron.

10 spots were investigated on the precorroded material. It must however be noted that the probing depth of the Raman analysis is estimated to be in the range of 0.5–1 μm [13]. A thin corrosion film of a different composition on the surface of the material could thus remain undetected if the bulk of the underlaying corrosion layer is composed of magnetite.

SEM analysis of a cross section of the precorroded iron foil embedded in carbon (Fig. 2), indicate that the corrosion layer appears to be uneven with some evidence of localized corrosion with a general oxide thickness in the order of a few μm up to about 10 μm.

3.2. Dynamics of immobilization

The concentrations of Se and U in the experimental solutions were measured as a function of reaction time (the analytical error is estimated to 1–10 μM). The results are displayed in Figs. 3 and 4. As the precorroded iron foils were transferred to the experimental solutions the redox potentials were found to stabilize in the range of −310 ± 30 mV vs SHE.

All solutions contained 10 mM NaCl and 2 mM $NaHCO_3$. The pH was measured and remained constant in the range of seven for samples 250SeIV/420U, 250SeVI/420U and ~8 for sample 250SeIV and 250SeVI. For sample 250SeVI no significant change in Se concentration is observed whereas the Se is slowly immobilized in sample 250SeIV (Fig. 3).

With uranyl (250SeIV/420U and 250SeVI/420U) the uranium was immobilized within 40 days (Fig. 4). The immobilization of the uranyl was associated with formation of a voluminous black corrosion product that was only weakly attached to the foils. The appearance of, or level of corrosion products on the samples without any uranyl (samples 250SeIV and 250SeVI) did not appear to change over the course of the experiment.

The selenite in sample 250SeIV/420U was completely immobilized within the same time frame as the uranyl (Fig. 4). The selenate in sample 250SeVI/420U decreased at a much lower rate reaching an apparent plateau level at ~125 μM, approximately half of the initial concentration (Fig. 4). We recently studied the influence of dissolved uranyl on the immobilization of selenate on a polished iron surface and on iron that was precorroded in a uranyl solution (anoxic conditions, similar surface areas, 10 mM NaCl, 2 mM $NaHCO_3$) [23]. In the present study the removal of selenate,

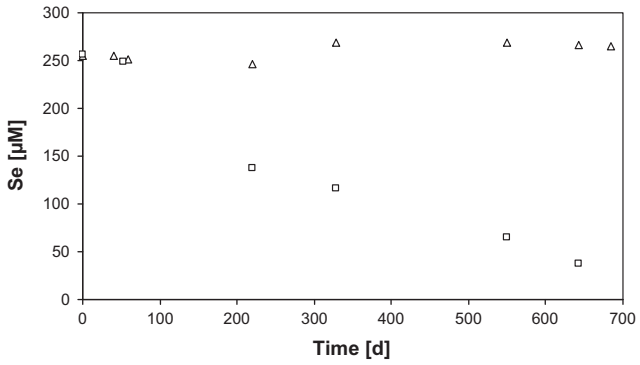

Fig. 3. Evolution of the Se concentration in samples SeIV250 (□) and SeVI250 (Δ).

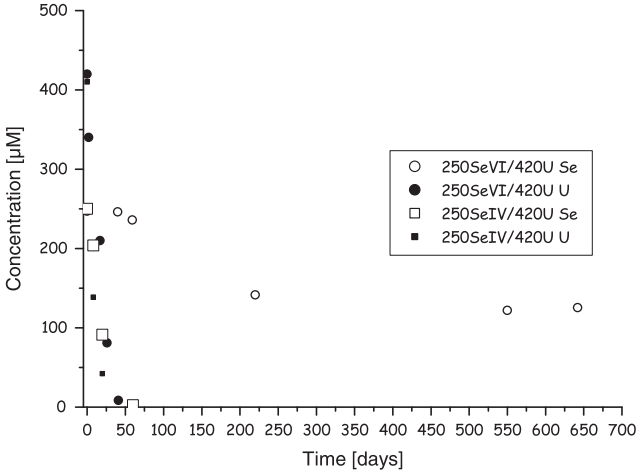

Fig. 4. Evolution of Se and U concentrations. Open symbols for Se concentrations and filled for U.

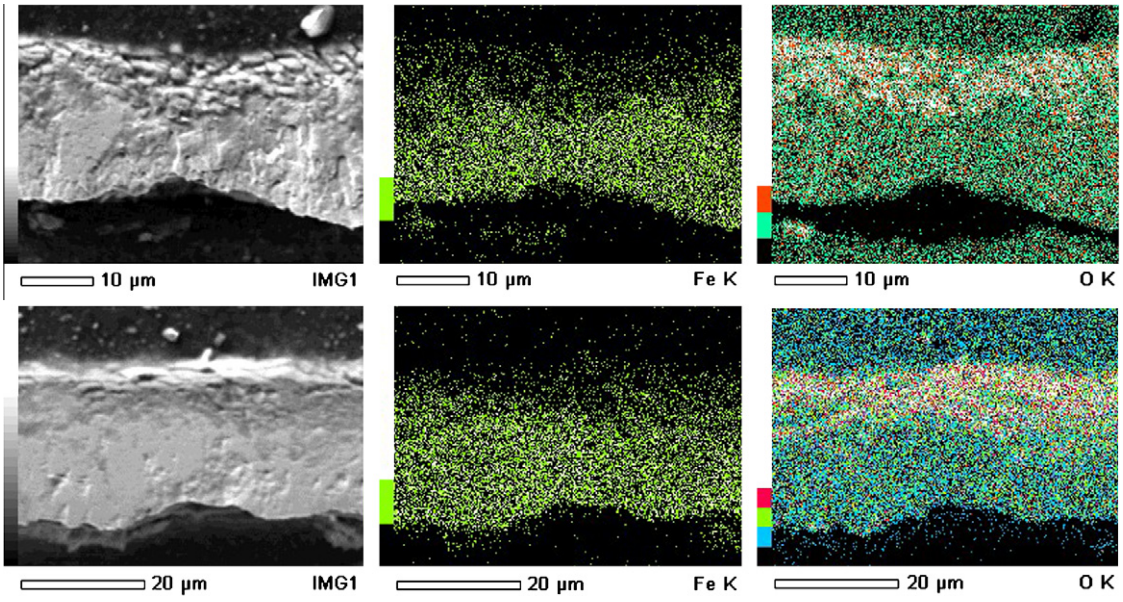

Fig. 2. SEM-EDS images of the cross section of a precorroded foil embedded in carbon.

and most notably, that of the uranyl is considerably slower. The lower immobilization rate in this study shows that the presence of the magnetite corrosion layer reduces the reactivity of the iron surface.

3.3. Characterization of the samples

BET measurements (Micromeritics Flowsorb II 2300, He/N_2: 70/30) of duplicate precorroded foils gives a surface area of ~0.1 m^2 per foil without any uranyl. After addition and subsequent immobilization of the equal amount of uranyl as in samples 250SeIV/420U and 250SeVI/420U the surface area increased to ~0.7 m^2. Small fractions of the experimental samples were removed after ~600 days. Raman spectroscopy indicates the presence of the iron corrosion product magnetite (strong band at 670 cm^{-1}) and maghemite (broad band at ~716 cm^{-1}) on the samples. Evidence of a very heterogeneous spatial distribution of elemental Se (Figs. 5 and 6) in samples 250SeIV/420U, 250SeVI/420U and 250SeIV is given by the band at 236 cm^{-1} corresponding to the stretching mode of trigonal zero-valent Se [27].

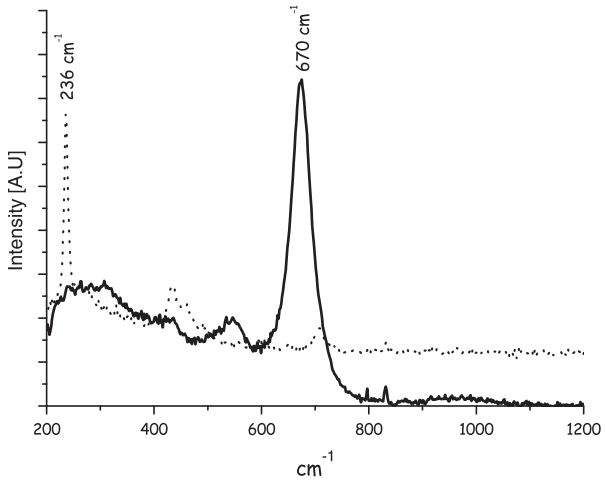

Fig. 5. Two Raman spectra from sample 250SeIV/420U.

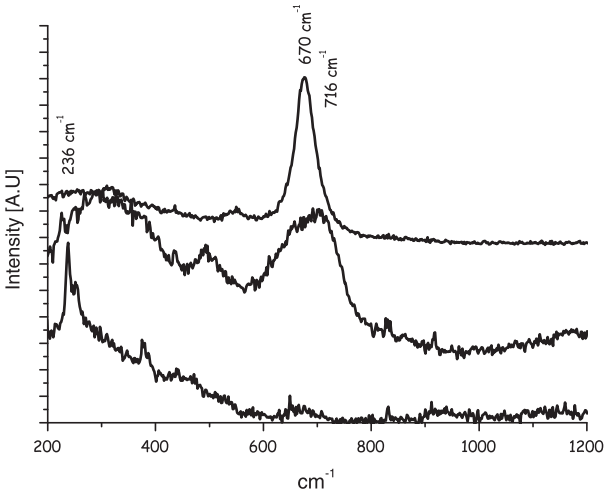

Fig. 6. Three Raman spectra from sample 250SeVI/420U.

Samples of the corrosion products formed in samples 250SeIV/420U, 250SeVI/420U and 250SeIV were allowed to dry inside the glove box, placed on a carbon tape and rapidly transferred to the SEM-EDS instrument for analysis. Acicular objects a few μm in length and <0.5 μm in diameter were identified in all samples (Figs. 7–10).

SEM-EDS mapping of the corrosion products from sample 250SeIV/420U gives an elemental distribution of ~40%-mass uranium, with the remainder being mostly iron and oxygen as well as a few percent selenium and a smaller fraction of carbon and sodium. Mapping of corrosion products from sample 250SeVI/420U gives very similar distributions with the possible difference that there is slightly less selenium. The uranium in the corrosion products from both samples appears to be rather homogenously distributed with no apparent hotspots and no indication of uranium rich crystals down to the resolution limit of the SEM-EDS (~0.1 μm).

The Se in the studied samples is strongly associated with the acicular objects (Figs. 7–10). In sample 250SeIV Se was also associated with spherical objects. Considering the Se Raman spectra of the samples and the documented formation of similar structures upon reduction of selenite they are most likely trigonal elemental Se crystals [28,29].

Micro X-ray Absorption Near Edge Structure (Micro XANES) spectroscopy was employed to investigate the speciation of Se and U on the samples. Representative selenium micro XANES spectra from the investigated samples and XANES spectra of reference compounds are presented in Fig. 11.

Using the energy of the absorption edge at half-height of the normalized XANES for the Se(VI), (IV), (0) and ferroselite, Se(−I) reference materials resulted in a perfectly linear correlation (R^2 = 0.9996) of the edge energy to the oxidation state. Assigned edge energies of samples and references can be found in Table 2. Definite assignment of the oxidation state of reduced Se species from XANES spectra is however difficult as non linear correlations are observed in several XAS studies of reduced selenium [10,11,30,31]. This behavior was also found for one of the candidate reference materials in this study, dioctyldiselenide Se(−I). The Se K edge has also been reported to be sensitive to varying degrees of crystallinity and different elemental allotropes [32]. The selenium on sample 250SeVI/420U do exhibit an edge shift to slightly lower energy and a reduced edge height compared to the

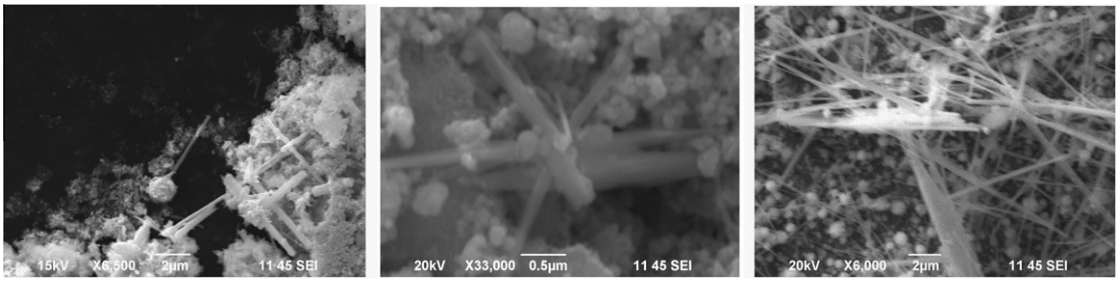

Fig. 7. SEM image of corrosion products on samples 250SeIV/420U (left), 250SeVI/420U (middle) and 250SeIV (right).

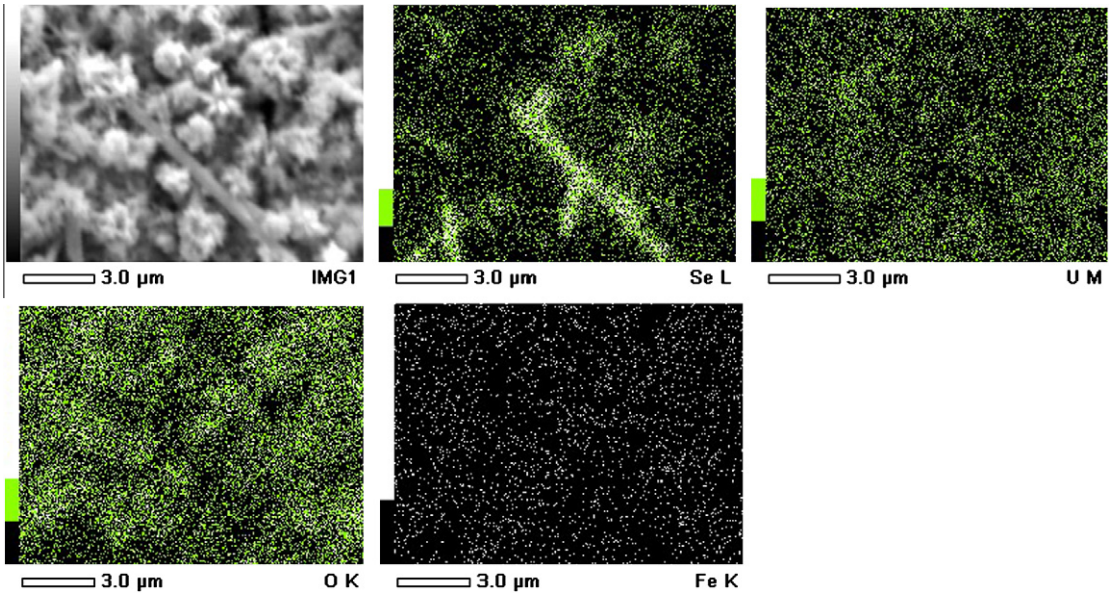

Fig. 8. SEM-EDS mapping around acicular objects in corrosion products from sample 250SeIV/420U.

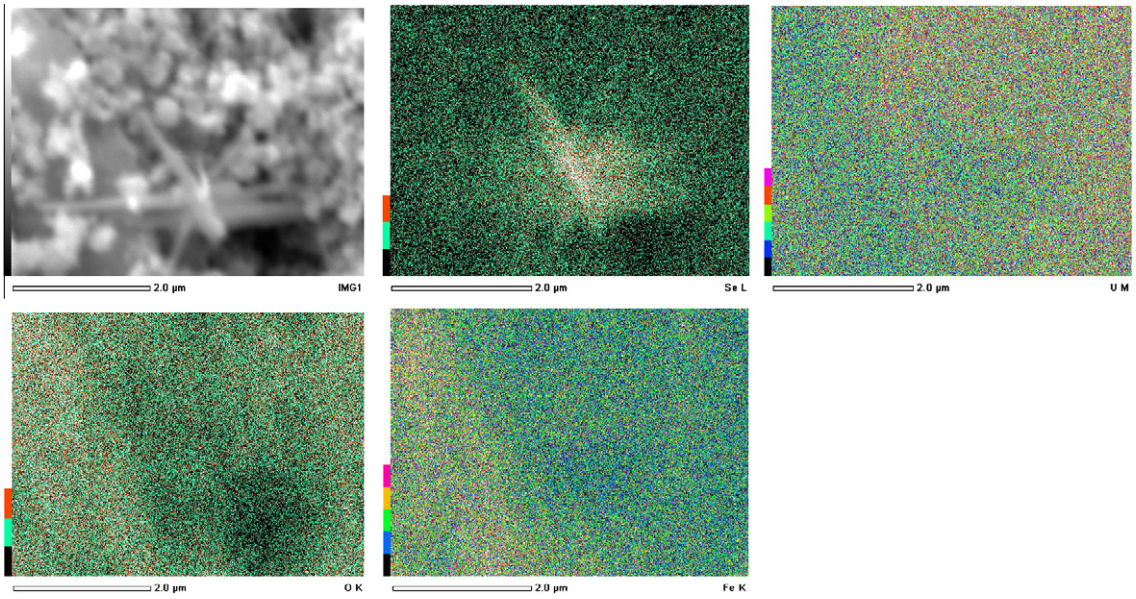

Fig. 9. SEM-EDS mapping around acicular objects in corrosion products from sample 250SeVI/420U.

elemental Se and ferroselite references. These features have similarities to those observed and assigned to FeSe or other Se(−II) containing ironselenides [11,15,32]. Given the uncertainty in the exact Se speciation and the possible mixed Se oxidation state in the range from elemental Se to Se(−II) we conclude that the immobilized Se was reduced to Se(0) or lower oxidation states (based on the Se-XANES and Raman data).

The speciation of the immobilized uranium on samples 250SeIV/420U and 250SeVI/420U was investigated using micro XANES (Fig. 12). Linear combination fits, LCF of the experimental micro XANES spectra with bulk XANES spectra of U(IV), UO_2 and U(VI), uranyl nitrate reference compounds revealed that the investigated uranium spots consisted of ~90% U(IV), i.e. the uranyl is largely reduced to U(IV) on the solid substrate. The LCF fits were processed using the Labview software package from beamline 10.3.2 [33].

No uranium species could however be detected by Raman spectroscopy despite the significant uranium content of up to ~40%-mass in the corrosion products (as determined by SEM-EDS). The absence of any discernable uranyl or cubic UO_2 bands in the Raman spectra combined with the U-XANES results of ~90% U(IV) leads us to the conclusion that the uranium is likely present as amorphous or nanocrystalline UO_2.

The precorroded iron foils with a magnetite layer appear to be inert towards selenate under the present conditions with no significant decrease in selenium concentration over 600 days (samples 250SeVI), despite the reducing conditions (redox potential ca −300 mV vs SHE). If reductive immobilization of selenate does not occur, this behavior is however not entirely unexpected given the small surface area and the limited selenate sorption capacity of magnetite at the pH ~8 [14]. The presence of uranyl and its subsequent immobilization by the corroded surfaces has a large impact

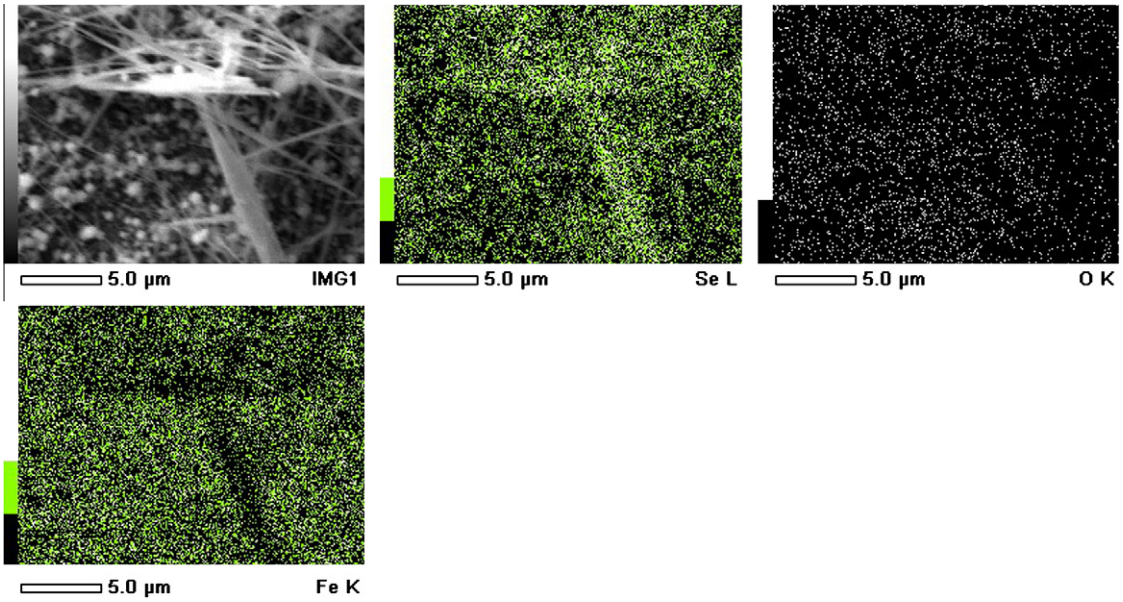

Fig. 10. SEM-EDS mapping around acicular objects on sample 250SeIV.

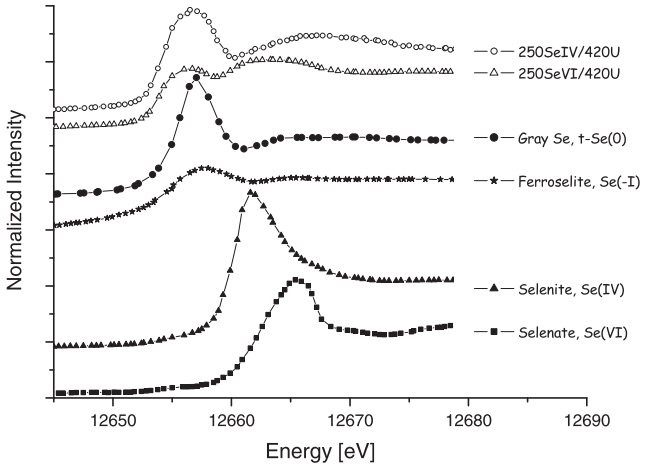

Fig. 11. Se-XANES spectra.

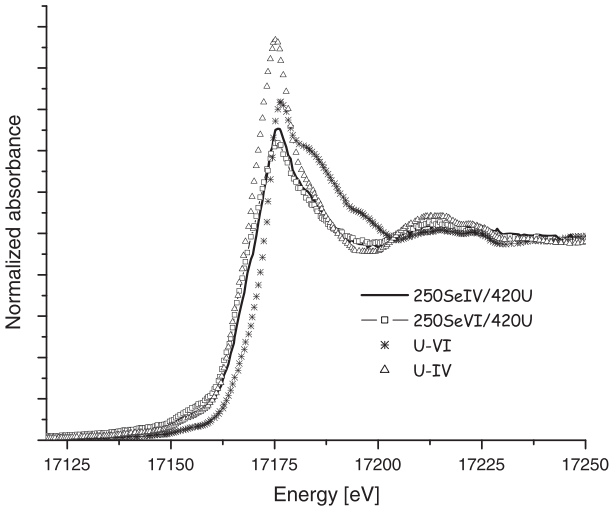

Fig. 12. U-XANES spectra.

on the reductive immobilization of dissolved selenate. The surface area does increase (by a factor of ~7 according to the BET measurement) and the pH is somewhat lower at ~7 when uranyl is present and being immobilized. But since no selenate is consumed in the sample without added uranyl the increased surface area from the reductive immobilization of uranyl does however not appear to fully explain the difference, particularly in the case of sample 250SeIV/420U were all selenite is immobilized. The uranyl facilitated reduction of selenate is considerably slower than that of the selenite and appears to stop after immobilization of ~50% of the selenate in solution. Given the standard potential for reduction of selenate to selenite ($SeO_4^{2-} + 3H^+ + 2e^- \rightarrow HSeO_3^- + H_2O$) of 1.075 V [35], with a calculated equivalent standard potential of ~0.45 V (using Nernst equation) at pH 7 there appears to be no thermodynamic explanation for this difference in immobilization. However, if intermediate Se(V) species are considered, data from the work of Kläning and Sehested [34], and our recent study [35] demonstrate that it takes either a two electron reductant or a stepwise reduction by a very strong one electron reductant to reduce selenate to selenite at the pH of the experiments (see Table 3). Whereas there are no reports of hindering intermediates for the reduction of selenite to Se(0).

Table 2
Assigned edge energies based on half-height of the normalized spectra.

Sample	Energy (eV)
Sodiumselenate, Se(VI)	12660.6
Sodiumselenite, Se(IV)	12658.5
Gray Selenium, Se(0)	12653.9
Ferroselite, Se (−I)	12652.6
Dioctyldiselenide, Se(−I)	12654.3
250SeVI/420U	12653.7
250SeIV/420U	12653.9
Uranylnitrate, U(VI)	17168.8
UO_2, U(IV)	17164.4
250SeIV/420U	17164.4
250SeVI/420U	17164.9

Table 3
Standard reduction potentials [34], and calculated equivalent reduction potentials at pH 7.

Standard process	E_0 (V)	Calculated E_0 at pH 7 (V)
$SeO_4^{2-} + 2H^+ + e^- \rightarrow SeO_3^{2-} + H_2O$	−0.03	−0.856
$SeO_3^- + H^+ + e^- \rightarrow HSeO_3^-$	2.18	1.767

Since oxidation of the magnetite layer would be expected to diminish its reductive capacity [36] the increased reductive selenium immobilization due to the uranyl reduction and precipitation is somewhat unexpected. A hypothesis is that the magnetite film is incapable of reducing selenate but that the reduction of uranyl by the magnetite surface promotes its dissolution exposing the underlying iron, and thereby facilitating the reduction of selenate. Uranyl has been shown to become reduced by magnetite [18], it has also been described that increasing the Fe(III) content of a magnetite film on iron promotes its dissolution [37]. By the dissolution of the passive layer the selenate can contact the iron surface or a more reactive underlying Fe(II)/Fe(III) oxide. Several workers have reported on the reduction of selenite and selenate by Fe(II) oxidized from zero-valent iron [6,15] as well as by green rusts [7], which are mixed Fe(II)/(III) hydroxides [38]. Carbonate-green rusts in particular have been identified to form under conditions similar to those in the experiments with uranyl [17].

Since only approximately half of the selenate is immobilized before the surface appears to become passive again we conclude that the uranyl induced breach in the passive film is transient. This can be rationalized by the observations that magnetite is among the iron oxides formed when selenate is reduced by Fe(II)/(III) oxyhydroxides [7,39], so that the surface in the present case repassivates itself towards selenate immobilization by reformation of a magnetite layer. Maghemite, γ-Fe_2O_3, another candidate passifying oxide which can form from the topotactic oxidation of the Fe(II) in magnetite was also observed by Raman spectroscopy in sample 250SeVI/420U (Fig. 6). The magnetite layer is however not passive with respect to uranyl and selenite immobilization. The passivity of magnetite towards selenate reduction is in line with the recent XAS-study of Kvashnina et al. [40] in which the selenium oxidation state was investigated on the surface of a polished and a precorroded iron surface after exposure to an anoxic selenate containing simulated groundwater solution. In that study the polished iron was found to reduce selenate to Se(−II), whereas the precorroded iron surface was only found to adsorb a very limited amount of selenate with no evidence of reduction. Although not mentioned in the paper [40], the iron oxide in the precorroded sample was identified (by Raman spectroscopy) as being composed of magnetite.

In order to investigate the proposed mechanism for the magnetite film breaking effect of uranyl, additional experiments were performed in the absence of selenite or selenate. Iron powder, precorroded under the same conditions as the iron foils were used. Fig. 13 shows the evolution of the corrosion products after addition of the uranyl solution (in 10 mM NaCl, 2 mM $NaHCO_3$, with ~10 times higher surface to volume ratio compared to the foil experiments with selenium). The uranyl was immobilized from solution within hours and within a few days a voluminous brownish precipitate formed on top of the corroded iron powder (represented by tube B, ~7 days in Fig. 13). As time passed the corrosion products settled and shifted towards a brown/greenish colour (tube C, ~21 days, Fig. 13). This layer slowly transformed over a few months into a black colour (tube D, ~90 days, Fig. 13). As can be seen in Fig. 14 the brownish corrosion product appearing after ~7 days was identified by Raman spectroscopy as lepidocrocite, γ-FeOOH based on the sharp strong band at 251 cm^{-1} and the broader bands at 213 cm^{-1} and 380 cm^{-1} [41]. The greenish product appearing after ~21 days was identified as a mixed Fe(II)/Fe(III) oxyhydroxide based on the broad signals at ~432 cm^{-1} attributed to Fe(II)–OH stretching and that of Fe(III)–OH at ~509 cm^{-1} [42,43]. Finally the black corrosion product forming after ~90 days was identified as magnetite by its band at 670 cm^{-1}. Based on these observations we propose that the uranyl is rapidly adsorbed by the magnetite film and then reduced into UO_2 over the course of a few days. In doing so the magnetite layer is oxidized into a voluminous γ-FeOOH precipitate leading to break down of the magnetite film. This accelerates the corrosion of the underlying iron surface leading to an increase in Fe(II) content and the transition of the γ-FeOOH into a mixed Fe(II)/Fe(III) oxyhydroxide (green rust). The green rust does however only appear to be a transient phase as magnetite is slowly reformed. These observations are in line with studies on the reaction of ferric oxyhydroxides (such as γ-FeOOH) and Fe(II) [44], including the observed formation of green rusts ([45], and references there in).

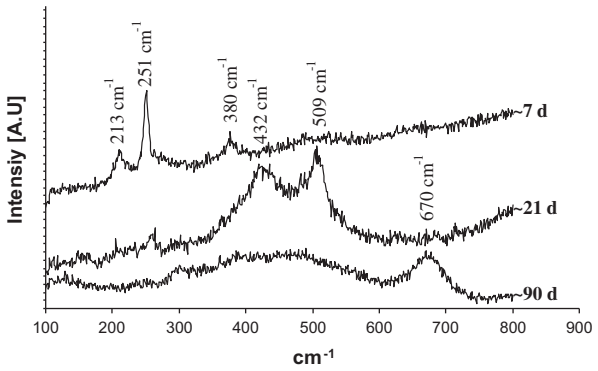

Fig. 14. Raman spectra of the evolution of the corrosion products in Fig. 13.

4. Conclusions

In the absence of uranyl, selenite was found to slowly become immobilized by the corroded (magnetite) surface predominantly yielding trigonal elemental Se crystals, whereas no immobilization of selenate took place. We propose that the barrier imposed by the reduction potential of intermediary Se(V) prevents reductive selenate immobilization by the magnetite surface. In the presence of

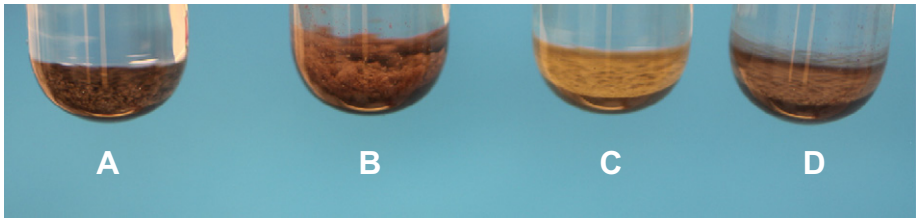

Fig. 13. Photograph of the evolution of precorroded iron powder after the uranyl addition. A: Precorroded iron powder. B: After ~7 days. C: After ~21 days. D: ~90 days.

uranyl being reduced by the magnetite covered iron surfaces we propose that the magnetite film is partially breached allowing the conduction of electrons or the outward diffusion of Fe(II) from the underlying iron, forming a more reactive Fe(II)/Fe(III) oxyhydroxide enabling the selenate immobilization, predominantly to elemental Se. Since only about half of the selenate in solution was immobilized, repassivation of the surface appears to occur. The observations in this study agree with our recent findings [23], that reduction of dissolved uranyl by a corroding iron surface greatly increase the reductive immobilization rate and capacity of the surface with regard to other dissolved contaminants such as selenate as well as selenite.

Acknowledgements

The Swedish Nuclear Fuel and Waste Management Co. (SKB) is gratefully acknowledged for financial support. Experimental assistance of the staff at the microXAS beamline, especially from Dr. Daniel Grolimund and Dr. Camelia Borca at the Swiss Light Source (SLS) is gratefully acknowledged.

References

[1] G. Jörg, R. Bühnemann, S. Hollas, N. Kivel, K. Kossert, S. Van Winckel, C. Lierse von Gostomski, Appl. Radiat. Isotopes (2010), doi:10.1016/j.apradiso.2010.05.006.
[2] A.L. Nichols, D.L. Aldama, M. Verpelli, Handbook of Nuclear Data for Safeguards. IAEA INDC(NDS)-0534, 2008.
[3] A. Fernández-Martinez, L. Charlet, Rev. Environ. Sci. Biotechnol. 8 (2009) 81–110.
[4] SKB-Technical Report. TR-06-22, 2006.
[5] A.P. Murphy, Ind. Eng. Chem. Res. 27 (1988) 187–191.
[6] Y. Zhang, J. Wang, C. Amrhein, W.T. Frankenberger Jr., J. Environ. Qual. 34 (2005) 487–495.
[7] S.C.B. Myneni, T.K. Tokunaga, G.E. Brown, Science 278 (1997) 1106–1109.
[8] S.R. Qiu, H.F. Lai, M.J. Roberson, M.L. Hunt, C. Amrhein, L.C. Giancarlo, G.W. Flynn, J.A. Yarmoff, Langmuir 16 (2000) 2230–2236.
[9] A.M. Scheidegger, D. Grolimund, D. Cui, J. Devoy, K. Spahiu, P. Wersin, I. Bonhoure, M. Janousch, J. Phys. IV: Proc. 104 (2003) 417–420.
[10] A.C. Scheinost, R. Kirsch, D. Banerjee, A. Fernandez-Martinez, H. Zaenker, H. Funke, L. Charlet, J. Contam. Hydrol. 102 (2008) 228–245.
[11] A.C. Scheinost, L. Charlet, Environ. Sci. Technol. 42 (2008) 1984–1989.
[12] N.R. Smart, D.J Blackwood, L. Werme, SKB-Technical Report TR-01-22, 2001.
[13] K. Ritter, M.S. Odziemkowski, R.W. Gillham, J. Contam. Hydrol. 55 (2002) 87–111.
[14] M. Martínez, J. Giménez, J. de Pablo, M. Rovira, L. Duro, Appl. Surf. Sci. 252 (2006) 3767–3773.
[15] R. López de Arroyabe Loyo, S.I. Nikitenko, A.C. Scheinost, M. Simonoff, Environ. Sci. Technol. 42 (2008) 2451–2456.
[16] O. Riba, T.B. Scott, K.V. Ragnarsdottir, G.C. Allen, Geochim. Cosmochim. Acta 72 (2008) 4047.
[17] D. Cui, K. Spahiu, Radiochim. Acta 90 (2002) 623–628.
[18] T.B. Scott, G.C. Allen, P.J. Heard, M.G. Randell, Geochim. Cosmochim. Acta 69 (2005) 5639.
[19] E.J. O'Loughlin, S.D. Kelly, R.E. Cook, R. Csencsits, K.M. Kemner, Environ. Sci. Technol. 37 (2003) 721–727.
[20] S.J. Morrison, D.R. Metzler, B.P. Dwyer, J. Contam. Hydrol. 56 (2002) 99–116.
[21] J.R. Muscatello, D.M. Janz, Sci. Total Environ. 407 (2009) 1318–1325.
[22] D. Nafts, S. Morisson, C. Fuller, J. Davies, Handbok of Groundwater Remediation Using Permeable Reactive Barries, 2002.
[23] A. Puranen, M. Jonsson, R. Dähn, D. Cui, J. Nucl. Mater. 392 (2009) 519–524.
[24] A.M. Scheidegger, D. Grolimund, M. Harfouche, M. Willimann, B. Meyer, R. Dähn, D. Gavillet, M. Nicolet, P. Heimgartner, Speciation, Techniques and Facilities for Radioactive Materials at Synchrotron Light Sources. NEA Publication No. 6046, 2006, pp. 81–86.
[25] T. Ressler, J. Synchrotron. Radiat. 5 (1998) 118–122.
[26] D.L.A. De Faria, S. Venâncio Silva, M.T. De Oliveira, J. Raman Spectrosc. 28 (1997) 873–878.
[27] V. Poborchii, A. Kolobov, K. Tanaka, Appl. Phys. Lett. 72 (1998) 1167–1169.
[28] C. An, S. Wang, Mater. Chem. Phys. 101 (2007) 357–361.
[29] F. Du, H. Wang, J. Mater. Sci. 42 (2007) 9476–9479.
[30] A. Ryser, D. Strawn, M. Marcus, J. Johnson-Maynard, M. Gunter, G. Möller, Geochem. Trans. 6 (2005) 1.
[31] M. Lenz, E.D. Van Hullenbusch, F. Farges, S. Nikitenko, C.N. Borca, P.N.L. Lens, Environ. Sci. Technol. 42 (2008) 7587–7593.
[32] I.J. Pickering, G.E. Brown, T.K. Tokunaga, Environ. Sci. Technol. 29 (1995) 2456–2459.
[33] M. Marcus, A.A. MacDowell, R. Celestre, A. Manceau, T. Miller, H.A. Padmore, R.E. Sublett, J. Synchrotron. Radiat. 11 (2004) 239–247.
[34] U.K. Kläning, K. Sehested, J. Phys. Chem. 90 (1986) 5460–5464.
[35] A. Puranen, M. Jansson, M. Jonsson, J. Contam. Hydrol. 116 (2010) 16–23.
[36] C.A. Gorski, J.T. Nurmi, P.G. Tratnyek, T.B. Hofstetter, M.M. Scherer, Environ. Sci. Technol. 44 (2010) 55–60.
[37] W.S. Li, J.S. Luo, Int. J. Electrochem. Sci. 2 (2007) 627–665.
[38] I.R. McGill, B. McEnaney, D.C. Smith, Nature 259 (1976) 200–201.
[39] H. Hayashi, K. Kanie, K. Shinoda, A. Muramatsu, S. Suzuki, H. Sasaki, Chemosphere 76 (2009) 638–643.
[40] K.O. Kvashnina, S.M. Butorin, D. Cui, J. Vegelius, A. Puranen, R. Gens, P. Glatzel, J. Phys. Conf. Ser. 190 (2009) 012191.
[41] S.J. Oh, D.C. Cook, H.E. Townsend, Hyperfine Interact. 112 (1998) 59–66.
[42] M. Reffass, R. Sabot, C. Savall, M. Jeannin, J. Creus, Ph. Refait, Corros. Sci. 48 (2006) 709–726.
[43] C.T. Lee, M. Odziemkowski, D.W. Shoesmith, J. Electrochem. Soc. 153 (2006) B33–B41.
[44] T. Ishikawa, Y. Kondo, A. Yasukawa, K. Kandori, Corros. Sci. 40 (1998) 1239–1251.
[45] C. Ruby, A. Aissa, A. Géhin, J. Cortot, M. Abdelmoula, J.-M.R. Génin, C.R. Geosci. 338 (2006) 420–432.